Performance of Coherent Detection in Optical Wireless Systems for High Speed Indoor Communications

Katerina Margariti and Thomas Kamalakis

Department of Informatics and Telematics, Harokopio University of Athens, Tavros, Athens GR17778, Greece

(Phone) 0030 2109549432, (Fax) 0030 2109549281, (E-mail) kmargariti@hua.gr

Abstract At a time of dramatically increasing bandwidth demand, the choice of the broadband technology adapted to future indoor applications, deserves serious consideration in the near term. Optical wireless technology goes beyond the capabilities of conventional radio communication systems and presents a realistic supplement to its counterpart. In this paper, a high-speed optical wireless communication system based on coherent reception technology is studied. Our analysis includes laser phase noise which, to the extent of our knowledge, has not been adequately addressed in the literature in the field of optical wireless. We also consider the influence of multipath-induced distortion. Our results indicate that coherent detection may significantly alleviate the power budget of line-of-sight and non-line-of-sight configurations. It can enable Gb/s wireless data transmission under moderate transmission powers consistent with eye safety regulations and the operational properties of optical transmitters typically found in the commercial marketplace.

Keywords *Coherent detection; laser phase noise; optical communications; wireless LAN*

1. INTRODUCTION

While much of the current debate over broadband communications largely revolves around the transition to the next generation of "last-mile" connectivity, telecom service providers, in response to the growing consumer demand for bandwidth and competitive pressures to differentiate their services, have well realized the need for bringing fiber networks ever closer to the home. Fiber to the home (FTTH) technologies, such as gigabit passive optical networks (GPON) promise gigabit-per-second bandwidth capability up to the customer's doorstep shifting broadband bottlenecks from access to the in-building network. A natural follow-up question is which technology will provide the "best-of-breed" solution for operators willing to take a long-term view toward broadband in-building network deployment. Wireline data distribution with multimode optical fibers can keep pace with growing network loads but comes at the expense of low terminal mobility, contributes to cable "spaghetti" and may require new cable installations in existing dwellings. On the wireless front, 802.11n is limited below 600Mb/s even when a multiple input multiple output (MIMO) configuration is used. With its 5-7GHz of license-free continuous bandwidth and the ensuing multi-Gbps throughput potential, 60GHz wireless systems are emerging as a high-speed alternative to WiFi for WLAN applications. Although the capabilities of the 60GHz system extend far beyond conventional wireless solutions in terms of capacity, major challenges still exist (Xia et al. 2007).

On the other hand, optical wireless (OW) technology provides unprecedented bandwidth potential, far in excess of any other wireless technology. In recent years, considerable research effort has been mobilized towards the realization of ultra-high speed short range optical wireless communications systems. To this direction, proof-of-concept experiments have been carried out incorporating line-of-sight (LOS) direct modulated (IM/DD) optical wireless systems operating at the infrared (IR) regime and it has been shown that gigabit per second communication can be achieved, supporting ~10Gb/s data rates (Wang et al. 2012), while 4x12.5Gb/s error-free operation can be provided when combined with WDM technology (Wang et al. 2011). Besides the vast available spectrum and the large data rates, optical wireless systems exhibit zero interference with existing radio systems and have negligible biological interaction. Link budget constraints posed by IM/DD optical wireless systems seems to be a "sore spot", pointing towards LOS architectures (O'Brien and Katz 2005), much like the case of 60GHz systems.

One way to improve this poor-link-budget barrier is to consider coherent detection technology that relies on the mixing of the received signal with a local oscillator (LO) carrier, providing additional gain at the receiver side. Over the past few years, coherent optical communications have witnessed a revival which has come about due to advancements ushered in the field of digital signal processing (DSP). To date, coherent detection has prove to be a cutting-edge technology, which allows a complete representation of the optical field into the electrical domain, providing intensity, phase, and polarization information from the incoming signal and improved spectral efficiency in fiber-based systems (Fludger et al. 2008).

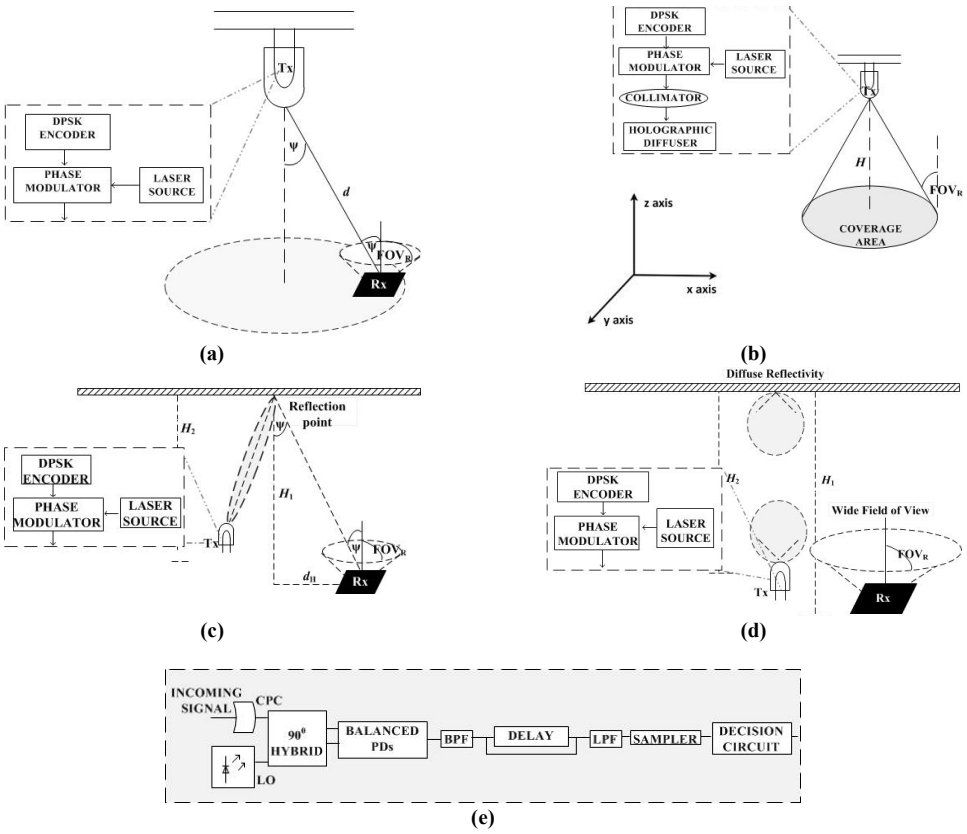

Fig.1 Building blocks of the various system architectures considered in the paper: a) directed LOS configuration b) non-directed LOS configuration incorporating a holographic diffuser element c) directed non-LOS (or hybrid) configuration d) non-directed non-LOS (or diffuse) configuration e) block diagram of the heterodyne coherent receiver. CPC stands for compound parabolic concentrator.

Moreover, due to the similarity between the coherent optical channel and the radio channel and more specifically the fact the optical phase information is retained, coherent detection can also open up intriguing possibilities using MIMO techniques (Ntogari et al. 2012), that promise to meet the growing demand for improved capacity and coverage of the system.

The benefits brought about by coherent detection seem substantial and well examined in the case of optical fiber-based systems. However, to the authors' knowledge, none of the previous research works have contributed a detailed framework in the case of wireless optical systems employing coherent detection since phase noise was ignored. In this paper, we investigate the potential of coherent detection in optical wireless systems by taking into account laser phase noise as well as thermal and shot noises. The distortion caused in both phase and amplitude of the received optical signal due to the multipath nature of propagation, is also considered in the case of a LOS system, assuming a room configuration where multipath-distortion is more pronounced. We provide a model for evaluating the system, based on Monte Carlo simulation, and we use this model to calculate the bit-error rate performance in terms of transmitted power and receiver placement. Encouraging results are obtained that can pave the way for future research towards the full exploitation of coherent technology virtues, such as improved spectral efficiency, more relaxed link-budgets, etc.

The remainder of this paper is structured in the following manner: Section 2 provides the theoretical framework that has been utilized for this study with respect to the antecedent theory and research findings. This section also addresses the different link topologies considered and provides with an overview of the system model. Section 3 gives a detailed account of a set of representative simulation results and a thorough discussion of the corresponding findings in the different scenarios considered. Finally, section 4 concludes this paper and provides motivation for further research in this area.

2. System Architecture &Model

2.1 System Configuration

Figure 1 shows the different system arrangements, along with the transmitter and receiver setup assumed. The phase modulator imprints the information in the phase of the laser beam. The choice of the laser diode (LD) as optical source is made due to the coherent nature of the emitted radiation which allows phase

recovery at the receiver. Eye and skin safety concerns pose strict limits on the amount of the transmitted optical power (Heatley et al. 1998) and in order to overcome these limitations, a holographic diffuser may be incorporated to ensure power safety in an indoor environment. The use of the holographic diffuser also results in a more uniform illumination and increased coverage area.

In this work we assume four different configurations illustrated in Fig. 1(a)-(d). In Fig. 1(a), a directed LOS link is shown that relies upon an unobstructed path between the transmitter and the receiver. Figure 1(b) shows a non-directed LOS link where a holographic diffuser is used for reasons discussed directly above. Figure 1(c) shows a directed non-LOS (or hybrid) link where there is no direct path between the transmitter and the receiver. A directional transmitter is placed at some height above the ground and the optical signal reaches the receiver after being reflected by the ceiling. Configurations employing narrow angle-of-view transmitters and receivers provide improved power budget and as a consequence high received optical power that come at the expense of limited coverage, higher blocking probability and strict alignment requirements. In order to achieve enhanced mobility and robustness against shadowing and blockage, a non-directed non-LOS (or diffuse) system setup should be considered. Such an arrangement employs a Lambertian-radiation-pattern transmitter along with a wide field-of-view receiver and the signal undergoes one or several reflections before reaching its destination. Within the context of this paper a single-bounce model is considered, where the transmitter and the receiver are placed at some height above the ground and pointed straight upward (Fig. 1(d)). Although in general diffuse configurations offer more robust optical links in terms of coverage, they suffer from poor link budget due to the increased attenuation associated with diffuse propagation and at the same time are impaired by multipath effects (Barry et al. 1993). To some extent, these effects can be compensated using equalization methods (Katz et al. 2006; Audeh et al. 1999).

Figure 1(e) illustrates the block diagram of the conventional differential phase-shift keying (DPSK) receiver structure considered in this paper. This standard delay-and-multiply type optical heterodyne binary-DPSK receiver has been analyzed previously (Barry and Lee 1990). The key element of the receiver is an optical 90^0 hybrid for mixing the incoming optical signal and an optical local oscillator (LO) signal, resulting in a signal at an intermediate frequency (IF) in the output ports of the coupler. In order to increase the sensitivity of the system and to fully utilize the received signal dual-balanced photo-detection is required. The produced photocurrent is mixed with a delayed replica of itself, using a delay line. A low-pass filter (LPF) removes remnants of the intermediate frequency and recovers the baseband signal. The resulting signal is sampled and led to the decision circuit.

2.2 Received Photocurrent

Based on the receive design shown in Fig. 1(e) assuming that the incoming optical signal envelope is $S = \sqrt{H(0)P_t}e^{j\varphi_k + j\theta(t)}$ and by subtracting the photocurrents from the two well-matched photo detectors, an expression for the resulting photocurrent is derived and given by (Barry and Lee 1990):

$$i(t) = 2R\sqrt{H(0)P_tP_{LO}}\cos\left(2\pi f_{IF}t + \varphi_k + \theta(t)\right) + n(t) \tag{1}$$

where $\varphi_k \in \{0,\pi\}$ represents the modulated phase of the k^{th} bit. Assuming a 2-level DPSK signal, the modulator introduces a phase shift equal to π between two consecutive pulses to be transmitted to represent digital bit "0", while the phase remains unaltered for digital bit "1". Hence, the phase difference between two adjacent pulses is given by:

$$\varphi_k - \varphi_{k-1} = \begin{cases} 0, & \text{"1"} \\ \pm\pi, & \text{"0"} \end{cases} \tag{2}$$

In (1), R is the responsivity of the photodetectors, $H(0)$ is the channel DC gain (determined by different relations according to the link configuration used and discussed in the following section), P_t is the transmitted optical power, P_{LO} is the LO optical power, $n(t)$ is an additive Gaussian noise component, which is due to the shot and thermal noise and $\theta(t)$ is the phase noise associated with the transmitter laser and the local oscillator.

2.3 Channel DC Gain

Provided that the distance between the transmitter and the receiver is much larger compared to the detector size, we may consider that the irradiance is constant over the surface of the detector. For most transmitters, the radiation pattern follows a generalized Lambertian model and the channel DC gain for a LOS optical wireless transmission system is given by (Barry et al. 1993):

$$H_{\text{LOS}}(0) = \frac{m+1}{2\pi d^2}(\cos^m\psi)A_{\text{eff}}\,\text{rect}\left(\frac{\psi}{\text{FOV}_{\text{R}}}\right) \tag{3}$$

where, referring to Fig. 1(a), ψ is the viewing angle with respect to the normal to the surface, which, under the specific arrangement, coincides with the angle of incidence relative to the receiver axis, FOV_{R} is the field of

view of the receiver and d is the distance between the transmitter and the receiver. The Lambertian order m is related to the transmitter's semiangle $\Phi_{1/2}$ through m=-ln2/ln(cos($\Phi_{1/2}$)) (Kahn and Barry 1997). The rectangular function is defined by:

$$\mathrm{rect}(x) = \begin{cases} 1, & x \geq 0 \\ 0, & x < 0 \end{cases} \tag{4}$$

and A_{eff} is the effective signal-collection area of the receiver. In the case when an ideal non imaging optical concentrator element with internal refractive index n is employed, A_{eff} is given by (Kahn and Barry 1997):

$$A_{\mathrm{eff}} = \begin{cases} A_{\mathrm{det}} \dfrac{n^2}{\sin^2(\mathrm{FOV_R})} \cos\psi, & 0 \leq \psi \leq \mathrm{FOV_R} \\ 0, & \psi > \mathrm{FOV_R} \end{cases} \tag{5}$$

where A_{det} is the physical detector area.

As mentioned previously, in order to be able to incorporate a high-performance emitter conforming to radiation safety standards, the laser system can be accompanied with a holographic diffuser to obtain nearly uniform illumination across the area covered. Assuming a lossless ideal holographic diffuser the channel DC gain is written as (Ntogari et al. 2012):

$$H_{\mathrm{HD}}(0) = \frac{A_{\mathrm{eff}}}{A_{\mathrm{cov}}} \tag{6}$$

where A_{eff} is determined by equation (5). The coverage area in (6), as depicted in Fig. 1(b) and under the condition that the viewing angle equals the field-of-view limit, is given by:

$$A_{\mathrm{cov}} = \pi H^2 \tan^2(\mathrm{FOV_R}) \tag{7}$$

where H is the vertical distance between the transmitter and the receiver.

In the directed non-LOS (or hybrid) arrangement (Fig. 1(c)) the channel DC gain is given by (Kahn and Barry 1997):

$$H_{\mathrm{HYBRID}}(0) = \begin{cases} \dfrac{\rho A_{\mathrm{det}} H_1 \cos\psi}{\pi \left(H_1^2 + d_{\mathrm{H}}^2\right)^{3/2}} \dfrac{n^2}{\sin^2(\mathrm{FOV_R})}, & \psi \leq \mathrm{FOV_R} \\ 0, & \psi > \mathrm{FOV_R} \end{cases} \tag{8}$$

where d_{H} and H_1 are the horizontal and vertical distance between the receiver and the reflection point, respectively and ρ the reflection coefficient of the ceiling.

Concerning the non-directed non-LOS (or diffuse) arrangement and following the analysis held in (Kahn and Barry 1997), where the field-of-view of the receiver (accompanied with a concentrator) is equal to $\pi/2$ the channel DC gain is given by:

$$H_{\mathrm{DIFFUSE}}(0) = \frac{\rho n^2 A_{\mathrm{det}} H_1^2 H_2^2}{\pi^2} \iint_{\mathrm{ceiling}} f(x,y)\,dx\,dy \tag{9}$$

The function $f(x,y)$ is defined as:

$$f(x,y) = \frac{1}{[(H_2^2 + (x-x_1)^2 + (y-y_1)^2)(H_1^2 + (x-x_2)^2 + (y-y_2)^2)]^2} \tag{10}$$

where H_1 and H_2 is the vertical distance between the receiver and the reflection point and between the transmitter and the reflection point, respectively (Fig. 1(d)), (x_1, y_1) and (x_2, y_2) the transmitter's and the receiver's coordinates, respectively, in the horizontal (x, y) plane.

2.4 Laser phase noise

Laser phase noise is considered a major impairment to the performance of coherent optical communication systems. This noise is caused by randomly occurring spontaneous emission events in the laser cavity and manifests itself as a random walk phase fluctuation of the laser output. The standard model is a continuous Brownian motion (Wiener-Lévy) process with Gaussian statistics (Atzmon and Nazarathy 2009). Due to the presence of phase noise, the power spectrum of the laser output diverges from the ideal profile of a delta function centered at the laser center frequency and a finite laser linewidth of a Lorentzian shape arises. In practice, coherent lightwave systems are evaluated in terms of their linewidth tolerance for a given bit rate (Kahn 2006).

There has been significant research effort towards the evaluation of the effect of laser phase noise on coherent fiber-based optical communication systems. The methods found in literature to define an analytic (or

semi-analytic) expression for the receiver's probability of error in the presence of phase and additive white Gaussian noise contributions may be grouped into two main categories. The first category is based on the perturbation analysis method, initially presented by Foschini and Vannucci (1988), for the probability density function of filtered phase noise, while the second analysis method is based on using the moments of random variables to either determine a bound on the receiver error probability or to indirectly compute the error probability through the estimation of the probability density function (pdf) of a noisy signal (Kaiser et al. 1993). The suitability of the above mentioned analysis methods, in terms of the range of phase noise levels and signal powers over which they are valid, for the case of an optical heterodyne binary DPSK receiver is also investigated in (Kaiser et al. 1993). Moreover, a simple analytic expression for the bit error rate (BER) with application to phase and differential phase shift keyed systems, based on the phase-noise exponent commutation concept, has been also derived (Atzmon and Nazarathy 2009).

In the context of this paper, a clear numerical approach has been utilized to define the error rate of the system assumed. The statistical properties of the phase noise introduced by transmit and LO lasers, as well as those of the additive noise contributions have been taken into account. This approach presents comparative advantage over the analytical / semi-analytical methods discussed in the previous paragraph, since it enables a more straightforward computation of the performance measures and allows a more accurate description of the properties of the associated subsystems / devices. As discussed above the phase noise $\theta(t)$ undergoes a Brownian-motion-type process and may be expressed by the following equation (Einarsson et al. 1993):

$$\theta(t) = 2\pi \int_0^t \mu(\tau) d\tau \tag{11}$$

where $\mu(t)$ is a zero mean white Gaussian noise with two-sided spectral density $R_\mu = \Delta\nu/2\pi$, and $\Delta\nu$ is the sum of the transmit and the LO laser linewidths. For modeling purposes, the phase noise $\theta(t)$ may be approximated in the discrete-time domain by the following relationship:

$$\theta(t) \cong \theta_d(t) = 2\pi\Delta\tau \sum_{i=1}^{N} \mu_i \tag{12}$$

where we have assumed that the duration $[0, t]$ is described by N samples located at $\tau_i = (i\text{-}1)\Delta\tau$ and $\Delta\tau$ is the sampling period. In (12), μ_i is the discrete version of $\mu(t)$. We assume that μ_i are independent identically distributed zero mean Gaussian random variables with variance σ_μ^2. It can be easily shown that since $\mu(t)$ is zero mean, $\theta(t)$ is also zero mean and the variance of $\theta(t)$ is calculated based on the following equation:

$$\begin{aligned} <\theta^2(t)> &= 4\pi^2 \int_0^t d\tau_1 \int_0^t d\tau_2 <\mu(\tau_1)\mu(\tau_2)> \\ &= 4\pi^2 \int_0^t d\tau_1 R_\mu = 4\pi^2 t R_\mu \end{aligned} \tag{13}$$

where we have substituted $\langle \mu(\tau_1)\mu(\tau_2) \rangle = R_\mu \delta(\tau_1 - \tau_2)$. We now need to make sure that the statistical properties of $\theta(t)$ and $\theta_d(t)$ are similar and hence we need to guarantee that their variance will also be equal. It is easy to see that the mean value of $\theta_d(t)$ is zero while its variance is given by

$$\begin{aligned} <\theta_d^2(t)> &\cong 4\pi^2 \sum_{i=1}^{N} \sum_{j=1}^{N} <\mu(\tau_i)\mu(\tau_j)> \Delta\tau_i \Delta\tau_j \\ &= 4\pi^2 \Delta\tau^2 \sum_{i=1}^{N} \sum_{j=1}^{N} <\mu(\tau_i)\mu(\tau_j)> \\ &= 4\pi^2 \Delta\tau^2 \sum_{j=1}^{N} <\mu^2(\tau_j)> = 4\pi^2 \Delta\tau^2 N \sigma_\mu^2 \end{aligned} \tag{14}$$

In order to have $\langle \theta_d(t)^2 \rangle = \langle \theta(t)^2 \rangle$ we need to choose σ_μ so that:

$$\sigma_\mu^2 = \frac{t R_\mu}{N \Delta\tau^2} = \frac{R_\mu}{\Delta\tau} = \frac{\Delta\nu}{2\pi\Delta\tau} \tag{15}$$

Equation (12) can be readily used to model the phase noise variations of the laser beams in the discrete time domain. In essence the phase $\theta(t)$ is approximated by $\theta_d(t)$ the latter being calculated by summing up a number of discrete "jumps" determined by the random variables μ_i. This approach allows us to incorporate the phase noise directly in our receiver model.

2.5 Additive noise components

The other noise sources that need to be considered is the shot noise and thermal noise which are modeled as additive white Gaussian noise contributions corresponding to the term $n(t)$ in equation (1). The power spectral densities for shot and thermal noise contributions are given below by equations (16) and (17), respectively (Green 1993).

$$N_{\text{shot}} = 2qR(H(0)P_t + P_{\text{LO}}) \tag{16}$$

$$N_{\text{thermal}} = \frac{2K_{\text{B}}T}{R_L} \tag{17}$$

where q is the electronic charge (1.6 10^{-19}C), K_{B} is the Boltzmann's constant (1.38 10^{-23} J/K), T is the absolute temperature (assumed T=300K throughout our calculations), and R_L is the load resistance.

2.6 Multipath-Induced Distortion

To account for multipath-induced distortion we consider the different signal components that arrive at the receiver via different transmission paths. The phases of the components vary randomly and hence the total signal may undergo power fluctuations. In addition, the phase of the received signal may also be distorted. To quantify these effects, we may write the received optical signal envelope S at the input of the coherent receiver as follows:

$$S = \sqrt{H(0)\,\mathrm{P}_t}\,e^{j\varphi_k + j\theta(\mathrm{t})} + \sum_{i=2}^{N} \sqrt{\mathrm{P}_i}\,e^{j\varphi_i^{'}} \tag{18}$$

where $H(0)$ represents the channel DC gain as expressed by equation (3), P_t represents the transmitted optical power, while P_i (for i >1) and $\varphi_i^{'}$ respectively represent the optical power and the phase of the components originating from multipath propagation. The interfering components can be thought as delayed replicas of the original signal and hence the phases $\varphi_i^{'}$, which include the phase changes due to the modulation, will correspond to previous bit intervals and therefore $\varphi_i^{'}$ can be assumed statistically independent. The power of the i^{th} interferer is calculated as:

$$P_i = P_t \int_{(i-1)T_b}^{iT_b} h(\tau)\partial\tau \tag{19}$$

where $h(t)$ is the impulse response of the channel and T_b is the bit period. Assuming also that the number of interferers N is large, then according to the central limit theorem (Rice 1995), S can be rewritten as:

$$S = \sqrt{H(0)\,\mathrm{P}_t}\,e^{j\varphi_k + j\theta(\mathrm{t})} + X + jY \tag{20}$$

where X and Y are independent zero mean normal random variables $X \sim N(0,\sigma^2)$, $Y \sim N(0,\sigma^2)$. It can be easily shown that the variance σ^2 is given by the following equation:

$$\sigma^2 = \frac{1}{2}\sum_{i=2}^{N} \mathrm{P}_i = \frac{1}{2}\int_{T_b}^{+\infty} h(\tau)\partial\tau \quad . \tag{21}$$

Under these assumptions, it is straightforward to show that, as in the case of conventional radio wireless systems, the magnitude $|S|$ of S follows a Rician distribution. However, since we use phase modulation, we are also interested in the phase variations of S due to the multipath effects and not just the variations in its amplitude. Therefore, in our simulations we have added the multipath effects by taking the photocurrent equation we have derived in the absence of multipath, as given in (1) and simply replacing $\sqrt{H(0)\,\mathrm{P}_t}$ with $|S|$ while at the same time accounting for the phase shift due to multipath interference. We therefore write the received photocurrent as:

$$i(t) = 2R|S|\sqrt{P_{LO}}\cos\left(2\pi f_{IF}t + \varphi_k + \theta(t) + \Delta\varphi\right) + n(t) \tag{22}$$

where we can easily show that $\Delta\varphi$ is the phase of $S\exp(-j\varphi_k - j\theta(t))$ which describes the variation of the received phase due to multipath interference.

2.7 BER Calculation

Based on the discrete time approach discussed in Section 2.2, we can apply a numerical method to compute the probability of error for the receiver. The photocurrent at the output of the balanced photodiodes (PDs) in Fig. 1(e) is written as:

$$i[p] = A\cos(2\pi f_{\mathrm{IF}} p\Delta\tau + \phi[p] + \theta_d[p]) + n[p] \tag{23}$$

where in the case where multipath effects are ignored, $A=2R[H(0)P_tP_{\mathrm{LO}}]^{1/2}$, $i[p]$ stands for $i(p\Delta\tau)$ and so forth, the additive noise contributions $n[p]$ (shot and thermal noise) are modeled as random variables with Gaussian distribution and power spectral densities given by equations (16) and (17), respectively. The model used to describe the phase noise $\theta_d[p]$, was given in previous section.

As shown in Fig. 1(e), the received photocurrent is fed to a band-pass filter (BPF), which we assume to be a fourth-order Butterworth filter, centered at the intermediate frequency f_{IF} in order to reduce unwanted noise. In our model, the output signal is the simply calculated by the inverse discrete Fourier transform (IDFT) of the product of the discrete Fourier transform (DFT) of the photocurrent, and the filter's transfer function. The output signal produced is multiplied by a replica of itself, delayed by one symbol period. In order to apprehend the heterodyne coherent decision mechanism operation, we may ignore, for the purposes hereof, the phase and additive noise contributions and result to the following simplified expression that describes the output of the delay line mixer:

$$\begin{aligned} u_s(t)u_s(t-T) = A_{DL}\{&\cos(\varphi_k - \varphi_{k-1} - w_{\mathrm{IF}}T) \\ &+ \text{double frequency terms}\} \end{aligned} \tag{24}$$

where $A_{DL} = \frac{R}{2}\sqrt{P_sP_{LO}}\left(\sin c(\omega_{IF}T/2)\right)^2$, P_s is the received optical power, w_{IF} is the intermediate angular frequency. For the case of heterodyne detection, the corresponding intermediate frequency resides within the gigahertz frequency band. In our model we have considered phase and additive noise contributions; however the underlying principles of operation remain the same. A low pass filter (LPF) with a Butterworth filter response, is used to filter out the undesired terms oscillating at $\pm 2f_{\mathrm{IF}}$ and further decrease noise. The output of the LPF is sampled every symbol period and fed into the decision circuit.

The decision circuit estimates the sign of the output signal, which stands for the sign of $\cos(\varphi_k - \varphi_{k-1})$ indicating in this way, the phase difference between successive pulses. In the presence of noise, the computed phase difference is compared with the corresponding phase difference of the signal initially sent and the number of errors is defined, through an exclusive or (XOR) logical operation. In this manner, one can numerically estimate the BER. To investigate the impact of multipath fading on the BER performance, we use again equation (23) but this time we take $A=2R|S|[P_{\mathrm{LO}}]^{1/2}$ and add a phase shift equal to $\Delta\varphi$ as discussed in the previous section. We generate normally distributed random variables X and Y with zero mean and variance given by equation (21). To estimate the impulse response $h(t)$ we use a previously developed modified Monte Carlo scheme (Ntogari et al. 2008; Lopez-Hernandez et al. 1998). Based on the values of X and Y, we calculate $|S|$ and $\Delta\varphi$ and then estimate the photocurrent and the BER accordingly.

3. Simulations and Discussion

3.1 Channel gain

The analysis presented in the previous section describes the theoretical and methodological aspects of the system under consideration and the models adopted to estimate its performance. Following this theoretical framework, our initial simulation results concern the study of the channel DC gain. The representative values of the parameters used along with the different configurations examined within this paper are gathered in Table I.

In the first setup where a direct LOS arrangement is considered, the transmitter is located at a fixed-point with coordinates (10, 10, 3), i.e. at the center of the ceiling. In this case, the parameter that will significantly affect the spatial power distribution as well the peak power value is the Lambertian radiation order m relating to the transmitter's semiangle at half power, as discussed in Section 2.3. In our simulations we have considered two different values of m, one representing a source that emits in a highly directional spatial intensity distribution (m=20) and the other corresponding to a broader radiation pattern (m=2). The spatial distribution of the channel DC gain for the direct LOS arrangement for the two different values of m is depicted in Fig. 2(a) and Fig. 2(b).

In order to distribute diffuse light uniformly over the coverage area, allowing class 1 eye safe operation for higher values of transmitted power a holographic optical element may be incorporated. In this case and according to Fig. 1(b), divergent light is converted into parallel beam of light through a collimating lens

TABLE 1

Simulation Parameters& Configurations for Indoor OW System

Parameter	Value Range			
Bit Rate	1Gbps			
Laser Wavelength	850nm			
Laser Linewidth	20MHz			
Intermediate Frequency	4GHz			
Room Dimension	20x20x3 m^3			
FWHM	15^0- 45^0			
FOV of the receiver	60^0			
Transmit Power	0.01 - 0.1mW (up to 5mW for non-directed configurations)			
LO Power	0.1-5mW			
Receiver Responsivity	1.0018 A/W			
Physical area of the PD	$1cm^2$			
Refractive index of the CPC	1.85			
Reflection coefficient (ceiling)	0.8			
3dB Bandwidth of BPF	10GHz			
Position & Orientation / Configuration	A	B	C	D
Transmitter				
x(m)	10	10	---	10
y(m)	10	10	---	10
z(m)	3	3	---	1.8
elevation	-90^0	-90^0	…	$+90^0$
Receiver				
x(m)	---	---	---	---
y(m)	---	---	---	---
z(m)	0.8	0.8	0.8	1.4
elevation	$+90^0$	$+90^0$	$+90^0$	$+90^0$

element and fed into the holographic diffuser mounted on the laser diode. According to equations (5), (6) and (7), the channel DC gain strongly depends on the receiver's field-of-view. Fig. 2(c) and Fig. 2(d) illustrate the spatial distribution of the channel DC gain for a non-directed LOS arrangement, incorporating a narrow and a wide field-of-view (FOV) detector, i.e. FOV=30^0 and FOV=60^0, respectively. As indicated from the graphical illustrations, a wider FOV provides an improved coverage but at the same time the received peak power is degraded by almost a factor of 25. A more accurate system model should also take into account the overall performance degradation caused by ambient light noise sources, more evident in the case of a wide FOV receiver. Moreover, in a practical system, a wide FOV receiver might also collect delayed replicas of the desired signal that have undergone two or more reflections along with the desired signal itself.

The third set up relies on a directed non-LOS (or hybrid) arrangement (Fig. 1(c)), where a directional transmitter is located at some height above the floor and pointing up towards the ceiling. The transmitted signal reaches the receiver after being reflected off the ceiling which is considered to have a reflection coefficient of 0.8. According to equation (8) the channel DC gain for a directed non-LOS link practically depends only on the distance between the reflection point and the receiver and not on the geometrical properties of the overall link topology, such as the distance between the transmitter and the receiver. The reflection point is considered at a fixed point with coordinates (10, 10, 3). By comparing the graphical illustrations of the channel DC gain spatial distributions for the directed LOS arrangement that employs a transmitter with a broader radiation pattern (Fig. 2(b)) and the directed non-LOS arrangement (Fig. 2(e)), we find that they exhibit similar coverage areas and a peak gain of the same order of magnitude. Since the reflected light is assumed to obey Lambert's cosine law and the ceiling exhibits a high diffuse reflectivity corresponding to a small reduction in the power of the reflected signal, this kind of behavior was expected to occur.

Fig. 2(f) displays the channel DC gain in the (x, y)-plane for the non-directed non-LOS (or diffuse) arrangement. In order to estimate the channel DC gain we integrated equation (9) numerically over a finite two-dimensional region representing the (x, y) dimensions of the room under consideration. For this calculation, we have assumed that a Lambertian source is placed at a fixed point with coordinates (10,10) in the horizontal plane and pointed straight up, while the receiver (having the same orientation as the transmitter) is set to move around the room on the horizontal plane. The transmitter-ceiling, receiver-ceiling vertical separations are set equal to H_2=1.2 and H_1=1.6m, respectively (Fig. 1(d)) and the ceiling is assumed to have reflectance of 80%. Although diffuse configurations are known to present several advantages over their LOS counterparts and hybrid configurations, such as less susceptibility to shadowing or blockage, from Fig. 2(f) it becomes evident that they exhibit the highest path loss and a significant decrease of the channel DC gain peak value of almost 20dB with respect to the directed LOS configuration incorporating a directional transmitter (Fig. 2(a)). A more accurate model than the single-bounce model considered here, should take into account the higher order reflections, that will lead, especially at large horizontal separations between the transmitter and the receiver (>5m), to a further almost 3dB decrease in the estimated path loss (Kahn and

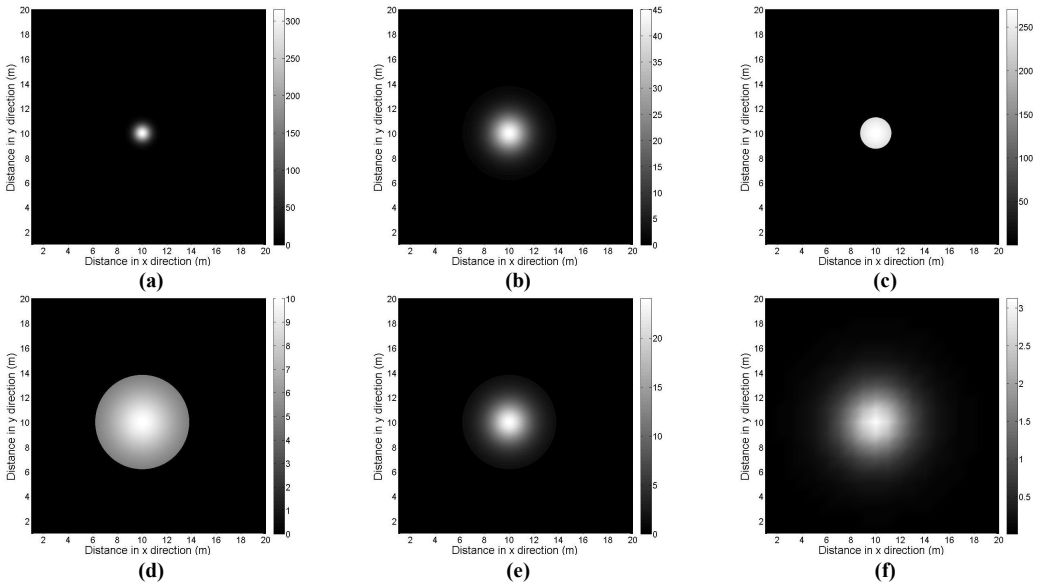

Fig. 2 Spatial distribution of the channel DC gain ($\times 10^{-6}$) for the different optical link configurations considered: a) directed LOS configuration incorporating a LD with Lambertian radiation order of m=20 and a 60^0 FOV receiver b) directed LOS configuration incorporating a LD with Lambertian radiation order of m=2 and a 60^0 FOV receiver c) non-directed LOS configuration incorporating a diffuser, with a 30^0 FOV receiver d) non-directed LOS configuration incorporating a diffuser, with a 60^0 FOV receiver e) directed non-LOS (or hybrid) configuration, with a reflection coefficient at the ceiling of 0.8 and a 60^0 FOV receiver f) non-directed non-LOS (or diffuse) configuration, based on the single-bounce approach, with a ceiling reflectance of 0.8 and a 60^0 FOV receiver

Barry 1997).

3.2 Receiver Sensitivity

Laser phase noise causes the system performance to be degraded. In order to gain a better understanding on its implications it is useful to evaluate its effect by ignoring all other noise sources (namely the additive component $n(t)$). Figure 3 provides a plot of the phase noise BER floor over a range of laser linewidth to system bit rate values calculated by our numerical model and out of 10^7 transmitted bits. The results are in good agreement with those obtained in (Kaiser et al. 1995) for the standard binary DPSK receiver. Given that the transmission bit rate is kept constant and equal to 1Gbps, varied BER floor values are basically obtained by setting different laser linewidth values. Figure 3 reveals that an acceptable BER performance of 10^{-3} (Wang et al. 2009) is obtained for laser linewidths up to 40 MHz, that are certainly within the range of commercially available lasers.

Taking into account the additive noise components as well, we calculate the required received optical power for a given performance level. The results are presented in Fig. 4 where we plot the BER as a function of the received power assuming various laser linewidths, and a constant LO power that equals 0.1mW. We confirm that even in the presence of shot and thermal noises, laser linewidths up to 40MHz can be used in order to obtain a BER value below 10^{-3} at -50dBm received power. Assuming a laser linewidth of 20MHz, the same BER performance is obtained at -60dBm suggesting that low receiver sensitivities can be obtained at 1Gbps data rates significantly relaxing link budget limitations, whereas an increase in the received power at -50dBm will allow nearly optimal performance (almost reaching BER floor) for the same value of laser linewidth.

3.3 Transmitted Power Requirements

The results shown previously can be extended to include channel loss thus enabling the analysis of the different system setups presented previously (Fig. 1). Initial results concern the numerical evaluation of the BER for different transmission power levels, as illustrated in Fig. 5. The results obtained involve 1Gbps data transmission for the different link topologies considered, incorporating a LD with a linewidth value in the order of 20MHz and a 60^0 field-of-view receiver. These configurations include: a) directed LOS transmission where a typical directed transmitter (Lambertian order m=20) is employed, b) non-directed LOS link incorporating a holographic diffuser element, c) directed non-LOS (or hybrid) transmission where the signal reflects off the ceiling with the reflection coefficient being 0.8 and d) non-directed non-LOS (or diffuse) link configuration, considering the single-bounce approach. The received power is obtained as the product of the corresponding channel DC gain, representing the path loss, and the transmit power. For the directed LOS, the non-directed LOS and directed non-LOS configurations, equations (3), (6) and (8), respectively, are used to

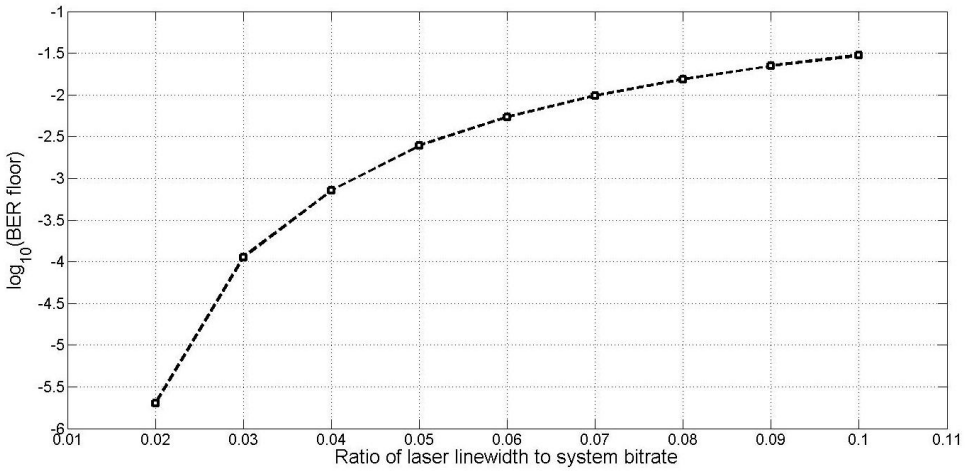

Fig. 3 BER floor as a function of the laser linewidth to system bit rate

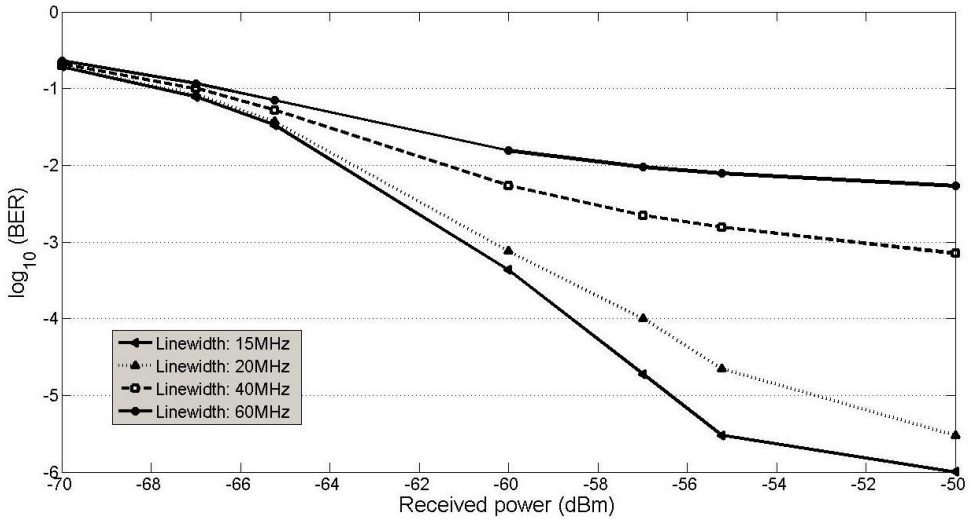

Fig. 4 BER as a function of the received power for different laser linewidth values

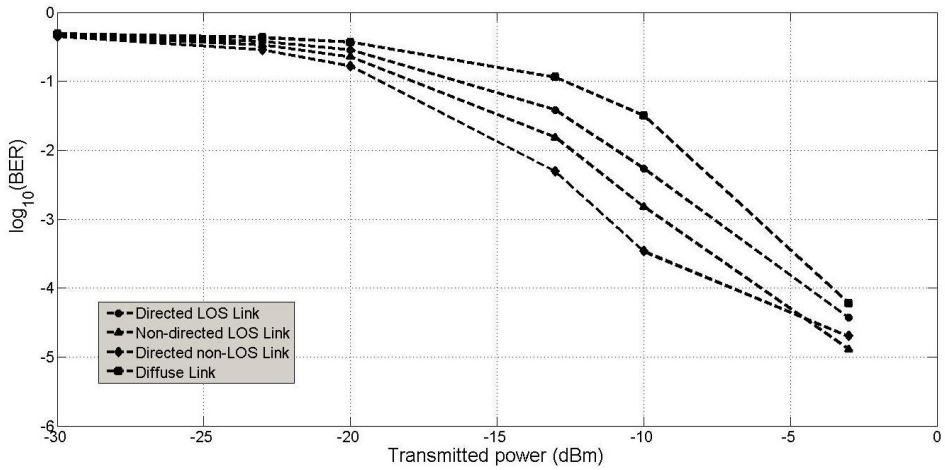

Fig.5 BER as a function of the transmission power. The results concern the different optical link configurations examined, namely directed LOS link, non-directed LOS link incorporating a diffuser, directed non-LOS (or hybrid) link, and non-directed non-LOS (or diffuse) propagation

calculate the channel DC gain. In either case, the horizontal distance between the transmitter and the receiver or between the transmitter and the reflection point for the directed non-LOS arrangement is set equal to 1m. The path loss for the non-directed non-LOS (or diffuse) configuration is set equal to -53dB, according to the results obtained in (Kahn et al. 1995) for a diffuse link setup modeled using the one-bounce approach,

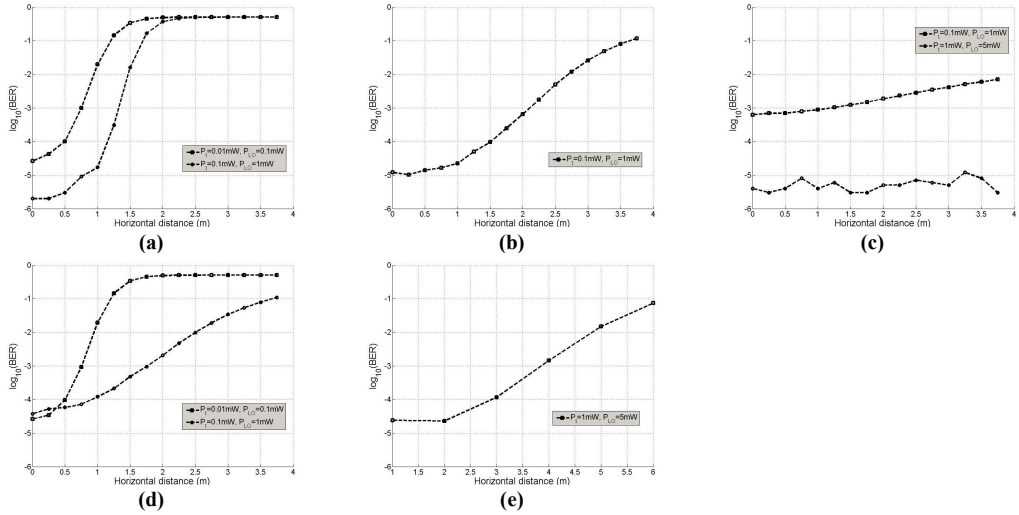

Fig. 6 BER as a function of the horizontal distance between the transmitter and the receiver a) directed LOS configuration, (Lambertian order m =20), for two different values of transmission and LO powers, b) directed LOS configuration (Lambertian order m=2), c) non-directed LOS configuration incorporating a diffuser for two different values of transmission and LO powers, d) directed non-LOS (or hybrid) configuration, for two different values of transmission and LO powers e) non-directed non-LOS configuration

corresponding to the path loss for 1m horizontal distance between the transmitter and the receiver. The path loss has been verified to be in a very good agreement with the corresponding value obtained by solving equations (9) and (10), for the same horizontal distance.

According to Fig. 5, and for the parameter values as defined in the previous paragraph, i.e. 1m horizontal distance between the transmitter (or the reflection point for the hybrid configuration) and the receiver and 20MHz transmit and LO laser linewidth, for transmitted power levels over the range of -30dBm to 20dBm the bit error rate value is kept at high levels for all the arrangements considered. As the transmission power increases, the bit error rate quickly falls down, to reach an acceptable value of 10^{-3} for transmitted power in the order of -11dBm and for the directed non-LOS arrangement. For the same value of BER, 5dB power penalty is observed between the directed non-LOS and the diffuse arrangements. At higher levels of emitted power, in the order of -3dBm the different arrangements exhibit a quite similar BER performance. Further increase in power is not feasible (in the case of directed optical wireless links) due to existing restrictions on radiation for safety concerns. In either case, the diffuse topology has the worst performance, in terms of the level of transmitted power required to achieve a given BER, when compared with the other arrangements. This kind of behavior was expected, since diffuse configurations offer more robust links at the expense of higher path losses.

3.4 Transceiver Placement

Figure 6 illustrates the BER as a function of the horizontal distance between the transmitter and the receiver for 1Gbps wireless optical transmission system incorporating a LD with a linewidth of 20MHz and a receiver with 60^0 FOV. Figure 6(a) illustrates the BER as a function of the transmitter – receiver horizontal distance for the directed LOS arrangement that incorporates a typical directed transmitter (m=20). Two graphs are provided corresponding to two different values of the transmitted and the LO powers. It becomes apparent that a tenfold increase in the launched optical power level delivers a tenfold improvement in the system bit error rate, as well an increase in the area covered. Figure 6(b) shows the same results assuming an emitter with less directive radiation pattern (m=2), 0.1mW transmission power and 1mW LO power. As expected the coverage area is extended but this comes at a cost of reduction in the peak value of the BER by almost one order of magnitude. By incorporating a holographic diffuser element, a more uniform distribution of the received optical power may be provided, as depicted in Fig. 6(c). Assuming 0.1mW transmission power and 1mW LO power, the bit error rate remains at an almost sufficiently level ($<10^{-3}$) for horizontal distances between the transmitter and the receiver of just up to1.2m. However, the incorporation of a holographic diffuser may allow a further increase in the transmit power, without concerns over the possible health effects from radiation exposure. By considering a transmit power level of 1mW and LO power of 5mW the BER will be maintained below the desired level of performance guarantee for almost 4m of horizontal distance.

Comparable results may be observed between the directed LOS configuration incorporating a transmitter with m=2 in Fig. 6(b) and the directed non-LOS transmission case in Fig. 6(d) for the same level of input power and LO power, namely 0.1mW and 1mW, respectively. This is expected since the latest configuration may be considered as a directed LOS configuration with a clear Lambertian radiation pattern (m=1) and a

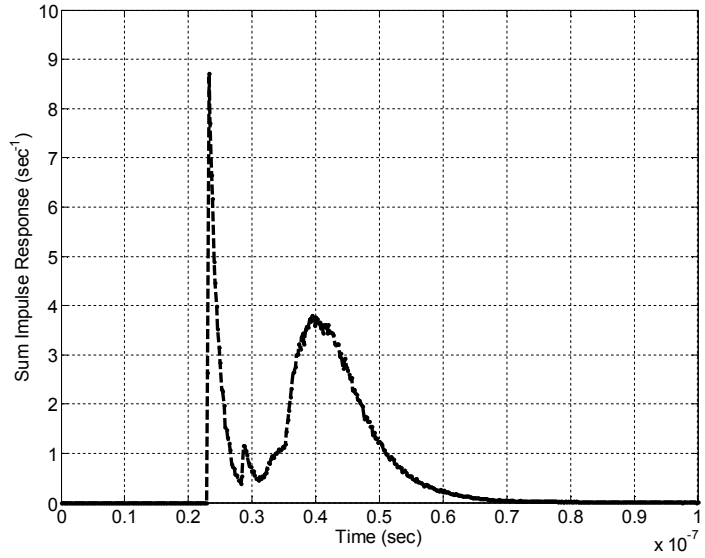

Fig.7 Channel impulse response for the examined configuration (Table 2), without taking into account the line-of-sight signal component

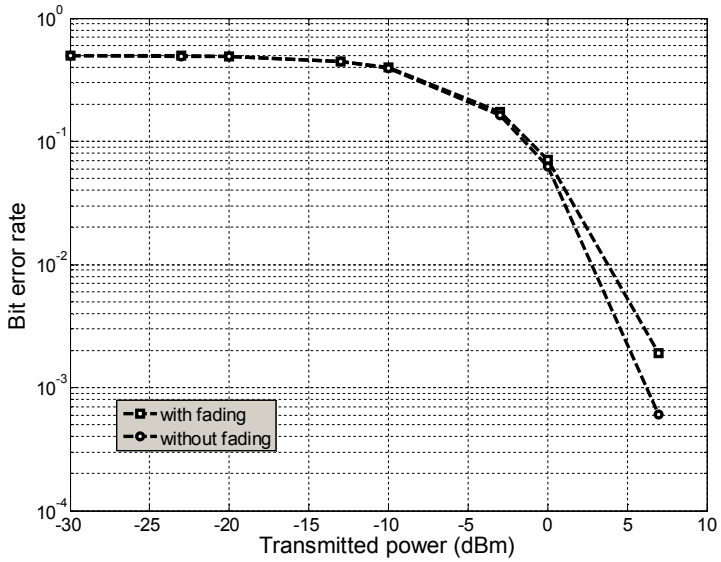

Fig.8 BER as a function of the transmitted power for 1Gbps wireless transmission. The results concern LOS configurations associated or not with multipath fading effects

decrease in the input power denoting the multiplication of the channel DC gain with the reflection coefficient of 0.8.

In the case of a diffuse link arrangement, where the transmit power may be raised to higher levels, for a transmit power in the order of 1mW and LO power in the order of 5mW, the BER is kept at an acceptable level for horizontal distance reaching almost 4m as shown in Fig. 6(e). The results are based on the single-bounce model used to characterize the channel and the corresponding path loss values estimated in (Kahn and Barry 1997). However, one should keep in mind that the specific results constitute only a rough estimation, since a more accurate model should include channel effects that will further hinder the system performance necessitating equalization schemes to mitigate for intersymbol interference (ISI).

3.5 System Performance Degradation due to Fading

In order to investigate the effects of multipath fading, we need to consider a smaller room such as the one considered by Barry et al. (1995), where no concentrator is used and multipath effects are more evident. The simulation parameters are as indicated in the following table, while the calculated channel impulse response (without the LOS component) is shown in Fig. 7. The power of the interfering components is calculated using (19). The results are presented in Fig. 8, where the BER is given as a function of the transmitted power with

TABLE 2

Simulation Parameters for Investigating Multipath Fading Effect

	Parameter	Values
Room:	(length, width, height) = (x,y,z)	(7.5m, 5.5m, 3.5m)
Source:	mode	1
	(length, width, height) = (x,y,z)	(2m, 4m, 3.3m)
	(elevation, azimuth)	$(-90^0,0^0)$
Receiver:	(A_{det}, FOV_R)	($1cm^2$, 70^0)
	(length, width, height) = (x,y,z)	(6.6m 2.8m 0.8m)
	(elevation, azimuth)	$(90^0,0^0)$

and without multipath induced distortion. In our calculations we have included the influence of the additive noise and the laser phase noise (assuming a linewidth of 20MHz). As indicated in Fig. 8, for the specific arrangement, multipath fading introduces a small power penalty. In situations where either the diffuse component σ^2 is more significant or there is no line-of-sight component to begin with, measures should be taken in order to mitigate the effect of fading through orthogonal frequency division modulation (OFDM) or diversity schemes (Belmonte and Kahn 2009).

4. Conclusion & Future Considerations

In this paper, we discussed the feasibility of coherent optical wireless links as a means to provide high capacity connections in an indoor environment. We have developed a model for analyzing the coherent optical wireless system forming a clear numerical method, as opposed to the analytical or semi-analytical approaches reported hitherto in the literature. Our model takes into account transceiver configuration along with its subsystems / components features and the statistical properties of additive and phase noise contributions. In all configurations, the use of coherent detection leads to low power requirements and this favorable link budget, provided even in non-line-of-sight arrangements, may be used to further increase the transmission rate. These results have arisen assuming that the characteristics of the components in use coincide with those commonly provided in the commercial sector, such as a 20MHz-linewidth laser, which underlines the practicality of the system under consideration. Achievable transmission rates on the order of Gbps have been reported, while LOS configurations associated with moderate-sized rooms appear robust against multipath induced distortion.

Coherent detection in optical wireless opens up a whole new set of research challenges and opportunities in the field of infrared communications and the wireless realm in general. The virtues brought about by technologies well documented in fiber-based and other conventional radio wireless systems, that enable considerable system performance improvement, are left to be investigated in optical wireless coherent systems. High spectral efficiency optical modulation formats, such as polarization multiplexed (PM) systems, wavelength division multiplexed (WDM) systems, optical frequency division multiplexing (OFDM) systems, that are also characterized by their immunity to multipath effects, as well as intersymbol interference (ISI) mitigation by electronic equalization, tracking and compensation of phase- and frequency offset, by algorithms performed in the digital domain may be also investigated for the case of optical wireless, taking into account all system characteristics and system impairments.

The results presented in this paper, along with the possibility to involve the above mentioned techniques, demonstrate the potential of coherent optical wireless systems in ultra-broadband corporate and home local area networks, as well as capacity-intensive data center applications.

Acknowledgements

The research reported in this paper was fully supported by the “ARISTEIA II” Action (“COWS” project) of the “Operational programme Education and Life Long Learning” and is co-funded by the European Social Fund (ESF) and the Greek state.

References

Atzmon, Y. and Nazarathy, M.: Laser Phase Noise in Coherent and Differential Optical Transmission Revisited in the Polar Domain. IEEE Journal of Lightwave Technology 27. 19-29 (2009)

Audeh, M. D., Kahn, J. M. and Barry, J. R.: Decision-Feedback Equalization of Pulse-Position Modulation on Measured Nondirected Indoor Infrared Channels. IEEE Transactions on Communications 47. 500-503 (1999)

Barry, J. R., Kahn, J. M., Krause, W. J., Lee, E. A. and Messerschmitt, D. G.: Simulation of Multipath Impulse Response for Indoor Wireless Optical Channels. IEEE Journal on Selected Areas in Communications 11. 367 – 379 (1993)

Barry, J. R. and Lee, E. A.: Performance of Coherent Optical Receivers. Proceedings of the IEEE 78. 1369 – 1394 (1990)

Belmonte, A. and Kahn, J. M.: Fundamental limits of diversity coherent reception on atmospheric optical channels. IEEE Conference Record of the Forty-Third Asilomar. Conference on Signals, Systems and Computers. 1621 – 1625 (2009)

Einarsson, G., Strandberg, J. and Monroy, I. T.: Error Probability Evaluation of Optical Systems Disturbed by Phase Noise and Additive Noise. IEEE Journal of Lightwave Technology 13. 1847 – 1852 (1995)

Fludger, C. R. S., Duthel, T., van den Borne, D., Schulien, C., Schmidt, E. –D., Wuth, T., Geyer, J., de Man, E., Khoe, G.-D., De Waardt, H.: Coherent Equalization and POLMUX-RZ-DQPSK for Robust 100-GE Transmission. IEEE Journal of Lightwave Technology 26. 64 – 72 (2008)

Foschini, G. J. and Vannucci, G.: Characterizing filtered light waves corrupted by phase noise. IEEE Trans. Info. Theory 34. 1437-1448 (1988)

Green, P.E., Jr.: Fiber Optic Networks. 1st edn. Prentice-Hall (1993)

Heatley, D. J. T., Wisely, D. R., Neild, I. and Cochrane, P.: Optical Wireless: The Story So Far. IEEE Communications Magazine 36. 72 - 74, 79-82 (1998)

Kahn, J. M.: Modulation and Detection Techniques for Optical Communication Systems. OSA Optical Amplifiers and Their Applications / Coherent Optical Technologies and Applications. Technical Digest (CD). CThC1 (2006)

Kahn, J. M. and Barry, J. R.: Wireless Infrared Communications. Proceedings of the IEEE 85. 265 – 298 (1997)

Kahn, J. M., Krause, W. J. and Carruthers, J. B.: Experimental Characterization of Non-Directed Indoor Infrared Channels. IEEE Transactions on Communications 43. 1613-1623 (1995)

Kaiser, C. P., Shafi, M. and Smith, P. J.: Analysis Methods for Opstical Heterodyne DPSK Receivers Corrupted by Laser Phase Noise. IEEE Journal of Lightwave Technology 11. 1820 – 1830, (1993)

Kaiser, C. P., Smith, P. J. and Shafi, M.: An Improved Optical Heterodyne DPSK Receiver to Combat Laser Phase Noise. IEEE Journal of Lightwave Technology 13. 525 – 533 (1995)

Katz, G., Sadot, D. and Tabrikian, J.: Electrical Dispersion Compensation Equalizers in Optical Direct- and Coherent-Detection Systems. IEEE Transactions on Communications 54. 2045-2050 (2006)

Lopez-Hernandez, J., Perez-Jimenez, R., and Santamaria, A.: Modified Monte Carlo scheme for high-efficiency simulation of the impulse response on diffuse IR wireless indoor channels. Electronics Letters 34. 1819 -1820 (1998)

Ntogari, G., Kamalakis T., and Sphicopoulos, T.: Performance Analysis of Non-Directed Equalized Indoor Optical Wireless Systems, IEEE 6th International Symposium on Communication Systems, Networks and Digital Signal Processing. CSNDSP08 Graz. 156 - 160 (2008)

Ntogari, G., Kamalakis, T., and Sphicopoulos, T.: Analysis of Indoor Multiple-Input Multiple-Output Coherent Optical Wireless Systems. IEEE Journal of Lightwave Technology 30. 317 – 324 (2012)

O'Brien, D. C. and Katz, M.: Optical wireless communications within fourth-generation wireless systems [Invited]. IEEE OSA Journal of Optical Networking 4. 312-322 (2005)

Rice J. A.: Mathematical Statistics and Data Analysis (Second edition). Duxbury Press, Belmont, C.A. (1995)

Wang, K., Nirmalathas, A., Lim, C., Skafidas, E.: Experimental Demonstration of a Full-Duplex Indoor Optical Wireless Communication System. IEEE Photonics Technology Letters 24. 188 – 190 (2012)

Wang, K., Nirmalathas, A., Lim, C., Skafidas, E.: 4x12.5 Gb/s WDM Optical Wireless Communication System for Indoor Applications. IEEE Journal of Lightwave Technology 29. 1988-1996 (2011)

Wang, Z. Zhong, W.-D., Fu, S., and Lin, C.: Performance Comparison of Different Modulation Formats Over Free-Space Optical (FSO) Turbulence Links With Space Diversity Reception Technique. IEEE Photonics Journal 1. 277-285 (2009)

Xia, P., Qin, X., Niu, H., Singh, H., Shao, H., Oh, J., Kweon, C. Y., Kim, S. S., Yong, S. K., Ngo, C.: Short Range Gigabit Wireless Communications Systems: Potentials, Challenges and Techniques. IEEE International Conference on Ultra-Wideband, 2007. ICUWB 2007. 123 – 128 (2007)